Generalized Morse Wavelets

Sofia C. Olhede and Andrew T. Walden, *Associate Member, IEEE*

***Abstract*—This paper examines the class of generalized Morse wavelets, which are eigenfunction wavelets suitable for use in time-varying spectrum estimation via averaging of time-scale eigenscalograms. Generalized Morse wavelets of order k (the corresponding eigenvalue order) depend on a doublet of parameters (β, γ); we extend results derived for the special case $\beta = \gamma = 1$ and include a proof of "the resolution of identity." The wavelets are easy to compute using the discrete Fourier transform (DFT) and, for $(\beta, \gamma) = (2m, 2)$, can be computed exactly. A correction of a previously published eigenvalue formula is given. This shows that for $\gamma > 1$, generalized Morse wavelets can outperform the Hermites in energy concentration, contrary to a conclusion based on the $\gamma = 1$ case.**

For complex signals, scalogram analyses must be carried out using both the analytic and anti-analytic complex wavelets or odd and even real wavelets, whereas for real signals, the analytic complex wavelet is sufficient.

***Index Terms*—Scalograms, spectrograms, time–frequency analysis, wavelet transforms.**

I. Introduction

THE continuous wavelet transform provides a method for analysis of a signal $x(t)$; working with a single, possibly complex-valued, wavelet function $\psi(t)$, we can consider the time-scale decomposition of a signal through the scalogram (modulus-squared of the continuous wavelet transform)

$$S(a,b) = \frac{1}{|a|}\left|\int_{-\infty}^{\infty} x(t)\psi^*\left(\frac{t-b}{a}\right)dt\right|^2$$

which expresses the energy of the signal at any scale $a > 0$ and time b. Here, $\psi^*(\cdot)$ denotes the complex conjugate of $\psi(\cdot)$.

Consider for a moment the field of spectrum analysis of stationary stochastic and/or noisy signals. Research has shown [1] that much can be gained by the following steps. A set of orthogonal data tapers is created, each giving rise to a different spectrum estimate. These spectrum estimates can then be averaged, and the resulting estimate is more interpretable since the variance is much reduced. The same general approach can be considered for scalogram estimation of stochastic and/or noisy signals. We wish to use several orthogonal wavelets from which we can create a set of different scalograms, which may be averaged together to produce a low variance scalogram estimate.

This paper considers the genesis and properties of a set of such orthogonal wavelets. We will approach the problem via solving a relevant eigenvalue problem and find *time-scale eigenscalograms*. An eigenscalogram is a scalogram, where the wavelet is an eigenfunction derived from a time/frequency concentration problem. For an eigenproblem, a set of orthogonal eigenfunctions are obtained, and we may label the first K of these, ordered by corresponding eigenvalue, as having "orders" $k = 0, \ldots, K-1$. Using these K eigenfunctions, a set of K eigenscalograms can be computed and averaged to produce the time-varying spectrum estimate.

A classical concentration problem is to look for the signal that loses the least energy after a truncation first in time and then in frequency, and the concentration region is the Cartesian product $[-T/2, T/2]\times[-B/2, B/2]$. The solutions (eigenfunctions) of the resulting eigenequation are the prolate spheroidal wave functions. Thomson [1] proposed the use of multiple discrete taper estimators of stationary spectra based on discrete prolate spheroidal sequences. Frazer and Boashash [2] extended Thomson's approach by segmenting the signal into quasistationary portions and computing the stationary spectrum estimator for each portion.

This energy concentration problem is posed "in two times one dimension," and a general joint time-frequency perspective should relate to "one times two dimensions" (see [3, p. 315]). Bayram and Baraniuk [4], [5] treated the concentration problem in this latter form, looking at time-varying spectrum estimation via averaging of *time-frequency eigenspectrograms* (a spectrogram being the modulus-squared of sliding-windowed complex sinusoids), using a set of Hermite eigenfunction windows derived in [6] and optimally concentrated in a region of the time–frequency domain.

Bayram and Baraniuk also looked at affine class time-scale eigenscalograms, using a set of Morse eigenfunction wavelets, which is discussed in [9] and optimally concentrated in a region of the time–frequency domain, excluding zero frequency. Generalized Morse eigenfunction wavelets of orders $k = 0, \ldots, K-1$ depend on the choice of a doublet of parameters (β, γ); when $\gamma = 1$, the zeroth-order wavelet is known as a Cauchy wavelet ([10, p. 29]). Bayram and Baraniuk concentrated on the Morse eigenfunction wavelets for $\beta = \gamma = 1$.

In this paper, we carefully analyze the generalized Morse wavelets (GMWs) for general β and γ. Section II reprises the time–frequency concentration problem for which the Hermite eigenfunctions are the solution and shows that the energy concentration of the operator in the specified domain is given by the *squares* of the eigenvalues and not the eigenvalues themselves (unlike in the prolate spheroidal wave function case). Section III proves the "resolution of identity" and derives the operator associated with the GMWs; the energy concentration is again given by the squares of the eigenvalues. The form of the eigenvalues of

Manuscript received December 14, 2001; revised June 18, 2002. The work of S. Olhede was supported by a Beit Scientific Research Fellowship, an EPSRC (UK) grant, and the Helge Axson Johnsons Stiftelse. The associate editor coordinating the review of this paper and approving it for publication was Dr. Xiang-Gen Xia.

The authors are with the Department of Mathematics, Imperial College of Science, Technology, and Medicine, London, UK.

Digital Object Identifier 10.1109/TSP.2002.804066.

the operator given here corrects the erroneous formula stated in [9, p. 680]. Most importantly, from a practical perspective, we show that the GMWs can outperform the Hermites in energy concentration when $\gamma > 1$; this is contrary to the conclusion in [5], which was based on the $\gamma = 1$ GMWs. The section concludes by noting that for each eigenvalue, λ_k, $k = 0, \ldots, K-1$, a pair of eigenfunctions (wavelets) are obtained, where one is an analytic function and the second its (anti-analytic) complex conjugate, and a computational method is given for their computation from the frequency-domain formula. Section IV is concerned with the fact that since the pair of wavelets can also be written as an even and an odd wavelet, two alternative orthogonal partitions of $L^2(\mathbb{R})$ are achieved. Evenness and oddness are also interpreted in terms of time direction through the continuous wavelet transform. For the special case of even and positive β and $\gamma = 2$, it is shown that the zeroth-order even wavelets can be found explicitly, in fact, in terms of Hermite polynomials and the odd wavelets by Hilbert transformation.

Section V is concerned with the effect of the orthogonal subspaces (even/odd or analytic/antianalytic) on the computation of time-scale *eigenscalograms*, which decompose the energy of the signal. It is shown that for real-valued signals, a scalar approach is sufficient, using only the analytic wavelet, whereas for complex-valued signals, a vector approach is needed, using wavelets from both subspaces. With the results of this paper, we conclude that the GMWs are a very useful multiple wavelet class with wide applicability (e.g., [11]).

A. Important Notation and Definitions

The inner product of two complex functions is given by $\langle x, y\rangle = \int_{\mathbb{R}} x^*(t)y(t)dt$, where * denotes the complex conjugate. We will need to work with both ordinary frequency and angular frequency; the Fourier transform of a function $x(t)$ in terms of frequency or angular frequency is here defined as $X(f) = \int_{\mathbb{R}} x(t)e^{-i2\pi ft}dt$ and $X(\omega) = \int_{\mathbb{R}} x(t)e^{-i\omega t}dt$, respectively. The inverse Fourier transform is given by $x(t) = \int_{\mathbb{R}} X(f)e^{i2\pi ft}df$, and $x(t) = (1/[2\pi]) \int_{\mathbb{R}} X(\omega)e^{i\omega t}d\omega$, respectively.

II. Time–Frequency Domains

A. Operator

In order to deal with domains that are more general than Cartesian products, Daubechies [6] used an approach based on localization operators, and similar results can be found by considering related operators [7], [8]. The "coherent state" associated with a point (s, f) in time–frequency space is $\phi_{s,f}(t) = e^{i2\pi ft}\phi(t-s)$. The choice $\phi(t) = \pi^{-1/4}e^{-t^2/2}$ (the Gabor wave function) attains the Heisenberg–Gabor inequality: $\phi_{s,f}(t)$ has the best localization around a point (s, f) and is used here. The following "resolution of identity" holds for $x(t) \in L^2(\mathbb{R})$

$$x(t) = \iint_{(s,f)\in\mathbb{R}^2} \phi_{s,f}(t)\,\langle\phi_{s,f}, x\rangle\, dsdf.$$

Restricting the signal to a domain $\mathcal{D}$ of time–frequency space defines the operator $x(t) \longrightarrow (\mathcal{P}_{\mathcal{D}}x)(t)$, where

$$(\mathcal{P}_{\mathcal{D}}x)(t) = \iint_{(s,f)\in\mathcal{D}} \phi_{s,f}(t)\,\langle\phi_{s,f}, x\rangle\, dsdf.$$

The ratio of the energy of the signal limited to the domain $\mathcal{D}$, $E_x(\mathcal{P}_{\mathcal{D}})$ to that of the original E_x is a real-valued quantity $\mu(\mathcal{D})$, say

$$\mu(\mathcal{D}) = \frac{E_x(\mathcal{P}_{\mathcal{D}})}{E_x} = \frac{\langle(\mathcal{P}_{\mathcal{D}}x), (\mathcal{P}_{\mathcal{D}}x)\rangle}{E_x}.$$

$\mathcal{P}_{\mathcal{D}}$ is positive and bounded by unity, and if $\mathcal{D}$ is bounded, then (see [6]) the operator is of trace class [12, pp. xvii, 37]. The operator is also self-adjoint, i.e., $\langle x, \mathcal{P}_{\mathcal{D}}y\rangle = \langle\mathcal{P}_{\mathcal{D}}x, y\rangle$, and therefore, by the Hilbert–Schmidt theorem [13, pp. 203, 209], there is a complete orthonormal basis $\{h_k(t)\}$ for $L^2(\mathbb{R})$ so that $(\mathcal{P}_{\mathcal{D}}h_k)(t) = \lambda_k h_k(t)$.

Then, any function $x(t) \in L^2(\mathbb{R})$ can be written

$$x(t) = \sum_{k=0}^{\infty} h_k(t)\,\langle h_k, x\rangle\,.$$

Let $x(t)$ have unit energy $E_x = \langle x, x\rangle = \sum_{k=0}^{\infty} |\langle h_k, x\rangle|^2 = 1$. As the spectrum of $\mathcal{P}_{\mathcal{D}}$ is purely discrete [6], we can order the eigenvalues in size $\lambda_0 \geq \lambda_1 \geq \cdots$. Then

$$\begin{aligned}\mu(\mathcal{D}) &= \left\langle \sum_{k=0}^{\infty} \langle h_k, x\rangle\,(\mathcal{P}_{\mathcal{D}}h_k)\,, \sum_{l=0}^{\infty} \langle h_l, x\rangle\,(\mathcal{P}_{\mathcal{D}}h_l)\right\rangle \\ &= \sum_{k=0}^{\infty}\sum_{l=0}^{\infty} \langle h_k, x\rangle^*\,\langle h_l, x\rangle\,\lambda_k\lambda_l\,\langle h_k, h_l\rangle \\ &= \sum_{k=0}^{\infty}\sum_{l=0}^{\infty} \langle h_k, x\rangle^*\,\langle h_l, x\rangle\,\lambda_k\lambda_l\delta_{k,l} \\ &= \sum_{k=0}^{\infty} |\langle h_k, x\rangle|^2\,\lambda_k^2 \leq \sum_{k=0}^{\infty} |\langle h_k, x\rangle|^2\,\lambda_0^2 = \lambda_0^2.\end{aligned}$$

Clearly, $\mu(\mathcal{D})$ is maximized for unit energy by taking $|\langle h_0, x\rangle|^2 = 1$ and $|\langle h_k, x\rangle|^2 = 0\ \forall k > 0$. Hence, $\mu(\mathcal{D})$ takes its maximum value of λ_0^2 for $x(t) = h_0(t)$ or a complex multiple thereof. If we want to find a function $x(t)$ that maximizes $\mu(\mathcal{D})$ while retaining the normalization $E_x = 1$ and such that $\langle h_k, x\rangle = 0$, $k = 0, \ldots, j-1$, then $x(t) = h_j(t)$ results, with $\mu(\mathcal{D})$ maximized at λ_j^2.

B. Hermite Eigenfunctions

When $\mathcal{D}$ corresponds to the disc of radius R about the origin in time-angular frequency space, i.e., $\mathcal{D}_R = \{(s, f) : s^2 + (2\pi f)^2 \leq R^2\}$, then the eigenfunctions take the form of scaled Hermite polynomials [6]. Given the first two Hermite polynomials $H_0(t) = 1$ and $H_1(t) = 2t$, subsequent ones can be generated from the recursion

$$H_{k+1}(t) = 2tH_k(t) - 2kH_{k-1}(t), \quad k \geq 1.$$

The orthonormal Hermite eigenfunctions take the form

$$h_k(t) = \frac{H_k(t)e^{-t^2/2}}{\pi^{1/4}\sqrt{[2^k\Gamma(k+1)]}}, \quad k = 0, 1, 2, \ldots \tag{1}$$

(see [14, p. 93]). The corresponding eigenvalues are in terms of the incomplete Gamma function $P(a,b) = \int_0^b y^{a-1}e^{-y}dy/\Gamma(a)$

$$\begin{aligned}\lambda_k(R) =& P\left(k+1, \frac{R^2}{2}\right) = \int_0^{R^2/2} \frac{y^k e^{-y}dy}{\Gamma(k+1)} \\ =& 1 - e^{-R^2/2}\sum_{j=0}^{k} \frac{2^{-j}R^{2j}}{j!}, \quad k = 0, 1, 2, \ldots\end{aligned}$$

where $\Gamma(\cdot)$ denotes the usual gamma function, and the final equality can be found in [15, eqn. 6.5.13].

If $\mathcal{D}$ corresponds to a disc of radius R about a point $(s_0, 2\pi f_0)$ in time-angular frequency space, then the eigenfunctions become $e^{i2\pi f_0 t}h_k(t - s_0)$, $k = 0, 1, 2, \ldots$.

III. Time-Scale Domains

A. Operator

We will now develop the more complicated framework of the generalized Morse wavelets. We begin with a version of the Cauchy wavelets [10, p. 29] given by ($p > 0$)

$$u_p(t) = \frac{2^p\Gamma(p+1)}{\sqrt{[\Gamma(2p+1)\pi]}}(1 - it)^{-(1+p)}$$

which has a Fourier transform of [16, eqn.3.382(7)]

$$U_p(\omega) = \begin{cases} \frac{2^{p+1}\sqrt{\pi}}{\sqrt{\Gamma(2p+1)}}\omega^p e^{-\omega}, & \text{if } \omega \in \mathbb{R}^+ \\ 0, & \text{otherwise.}\end{cases}$$

Now, we introduce parameters $\gamma \geq 1$, $\beta > (\gamma - 1)/2$ and let $r = (2\beta+1)/\gamma$. First, define a weight function $\eta(\omega)$ associated with a change of variables by

$$\eta(\omega) = \left[\frac{d}{d\omega}(|\omega|^{\gamma-1}\omega)\right]^{1/2} = |\omega|^{(\gamma-1)/2}\sqrt{\gamma}$$

and, second, the frequency domain function

$$\begin{aligned}V^{(\beta,\gamma)}(\omega) =& U_{(r/2)-(1/2)}\left(|\omega|^{\gamma-1}\omega\right)\eta(\omega) \\ =& \begin{cases} \frac{2^{r/2+1/2}\sqrt{[\pi\gamma]}}{\sqrt{\Gamma(r)}}|\omega|^\beta e^{-\omega|\omega|^{\gamma-1}}, & \text{if } \omega \in \mathbb{R}^+ \\ 0, & \text{otherwise.}\end{cases}\end{aligned}$$

It follows from [16, sec.3.478(1)] that

$$\int_{\mathbb{R}^+}\left|V^{(\beta,\gamma)}(\omega)\right|^2 d\omega = 2\pi \quad \text{or} \quad \int_{\mathbb{R}^+}\left|V^{(\beta,\gamma)}(f)\right|^2 df = 1. \tag{2}$$

Let us introduce translation and dilation parameters b and $\tilde{a} \in \mathbb{R}$, respectively. (When the dilation parameter can only be positive we will denote it by $a \in \mathbb{R}^+$.) Now, we have (3), shown at the bottom of the page.

In addition

$$\begin{aligned}V^{(\beta,\gamma)}_{\tilde{a},b}(\nu) =& |\tilde{a}|^{1/(2\gamma)}e^{-ib\nu|\nu|^{\gamma-1}}V^{(\beta,\gamma)}\left(|\tilde{a}|^{(1/\gamma)-1}\tilde{a}\nu\right) \\ =& \int_{\mathbb{R}} |\tilde{a}|^{1/(2\gamma)}e^{-ib\nu|\nu|^{\gamma-1}}u_{(r/2)-(1/2)}(\tau) \\ & \cdot e^{-i\tau\tilde{a}\nu|\nu|^{\gamma-1}}\eta\left(|\tilde{a}|^{1/\gamma}\nu\right)d\tau \\ =& \int_{\mathbb{R}} \frac{1}{\sqrt{|\tilde{a}|}}u_{(r/2)-(1/2)}\left(\frac{\tau - b}{\tilde{a}}\right) \\ & \cdot e^{-i\tau\nu|\nu|^{\gamma-1}}\eta(\nu)d\tau.\end{aligned}$$

Note that

$$V^{(\beta,\gamma)}_{-\tilde{a},-b}(\nu) = V^{(\beta,\gamma)}_{\tilde{a},b}(-\nu). \tag{4}$$

Let $v^{(\beta,\gamma)}_{\tilde{a},b}(t)$ denote the inverse Fourier transform of $V^{(\beta,\gamma)}_{\tilde{a},b}(\nu)$. Then

$$v^{(\beta,\gamma)}_{\tilde{a},b}(t) = \int_{\mathbb{R}} \frac{1}{\sqrt{|\tilde{a}|}}u_{(r/2)-(1/2)}\left(\frac{\tau - b}{\tilde{a}}\right)L(\tau, t)d\tau$$

where

$$L(\tau, t) = \frac{1}{2\pi}\int_{\mathbb{R}}\left\{\eta(\nu)e^{-i\nu(\tau|\nu|^{\gamma-1}-t)}d\nu\right\}d\tau.$$

Therefore, $L(\cdot,\cdot)$ is a function that transforms the time parameter, and after this transformation has taken place, our new time variable is dilated and translated. Note that when $\gamma = 1$, time is not altered before scaling and translating. Furthermore

$$\begin{aligned}&\int_{\mathbb{R}}\left|v^{(\beta,\gamma)}_{\tilde{a},b}(t)\right|^2 dt \\ &\qquad = \begin{cases} \frac{1}{2\pi}\int_{\mathbb{R}^+}\left|V^{(\beta,\gamma)}_{\tilde{a},b}(\nu)\right|^2 d\nu & \text{if } \tilde{a}, \nu \in \mathbb{R}^+ \\ \frac{1}{2\pi}\int_{\mathbb{R}^-}\left|V^{(\beta,\gamma)}_{\tilde{a},b}(\nu)\right|^2 d\nu & \text{if } \tilde{a}, \nu \in \mathbb{R}^-. \end{cases}\end{aligned} \tag{5}$$

and from (2) and (3), we see that $v^{(\beta,\gamma)}_{\tilde{a},b}(t)$ has norm unity.

The following "resolution of identity" holds for $x(t) \in L^2(\mathbb{R})$:

$$x(t) = C_0 \iint_{(\tilde{a},b)\in\mathbb{R}^2} v^{(\beta,\gamma)}_{\tilde{a},b}(t)\left\langle v^{(\beta,\gamma)}_{\tilde{a},b}, x\right\rangle \tilde{a}^{-2}d\tilde{a}\,db \tag{6}$$

$$\begin{aligned}V^{(\beta,\gamma)}_{\tilde{a},b}(\nu) =& |\tilde{a}|^{1/(2\gamma)}\,e^{-ib\nu|\nu|^{\gamma-1}}V^{(\beta,\gamma)}\left(|\tilde{a}|^{(1/\gamma)-1}\,\tilde{a}\nu\right) \\ =& \begin{cases} \frac{2^{(r/2)+(1/2)}\sqrt{[\pi\gamma]}|\tilde{a}|^{r/2}}{\sqrt{\Gamma(r)}}|\nu|^\beta e^{-(\tilde{a}+ib)\nu|\nu|^{\gamma-1}}, & \text{if } \tilde{a}\nu \in \mathbb{R}^+ \\ 0, & \text{otherwise.}\end{cases}\end{aligned} \tag{3}$$

where $C_0 = (2\beta + 1 - \gamma)/(4\gamma\pi)$. This is proved in the Fourier transform domain, i.e., we show in the Appendix that

$$X(\nu) = C_0 \iint_{(\tilde{a},b)\in\mathbb{R}^2} V_{\tilde{a},b}^{(\beta,\gamma)}(\nu) \left\langle V_{\tilde{a},b}^{(\beta,\gamma)}, X \right\rangle \tilde{a}^{-2} d\tilde{a}\, db. \quad (7)$$

Consider a symmetric bounded set $\tilde{\mathcal{A}}$ of $\mathbb{R}^2$. Using the correspondence

$$\tilde{a} = C_1^{\gamma} [2\pi|f|]^{-\gamma} \operatorname{sign}(f);\ b = C_2^{-1} s|\tilde{a}|^{1-(1/\gamma)}$$

for constants C_1 and C_2, which will be defined later, we have

$$(\tilde{a}, b) \in \tilde{\mathcal{A}} \iff (s, f) \in \tilde{\mathcal{D}}$$

and define the operator $\mathcal{P}_{\tilde{\mathcal{D}}}$, where $x(t) \longrightarrow (\mathcal{P}_{\tilde{\mathcal{D}}} x)(t)$, by

$$(\mathcal{P}_{\tilde{\mathcal{D}}} x)(t) = C_0 \iint_{(\tilde{a},b)\in\tilde{\mathcal{A}}} v_{\tilde{a},b}^{(\beta,\gamma)}(t) \left\langle v_{\tilde{a},b}^{(\beta,\gamma)}, x \right\rangle \tilde{a}^{-2} d\tilde{a}\, db.$$

The positive self-adjoint operator is trace class since if we take any basis $\{\psi_l\}$ of $L^2(\mathbb{R})$, then for finite $\tilde{\mathcal{D}}$

$$\begin{aligned}\sum_l \langle \psi_l, \mathcal{P}_{\tilde{\mathcal{D}}} \psi_l \rangle &= C_0 \iint_{(\tilde{a},b)\in\tilde{\mathcal{A}}} \sum_l \left| \left\langle v_{\tilde{a},b}^{(\beta,\gamma)}, \psi_l \right\rangle \right|^2 \tilde{a}^{-2} d\tilde{a}\, db \\ &= C_0 \iint_{(\tilde{a},b)\in\tilde{\mathcal{A}}} \left| \left\langle v_{\tilde{a},b}^{(\beta,\gamma)}, v_{\tilde{a},b}^{(\beta,\gamma)} \right\rangle \right|^2 \tilde{a}^{-2} d\tilde{a}\, db \\ &= C_0 \iint_{(\tilde{a},b)\in\tilde{\mathcal{A}}} \tilde{a}^{-2} d\tilde{a}\, db \\ &= \frac{(2\beta + 1 - \gamma)}{2C_1C_2} \iint_{(s,f)\in\tilde{\mathcal{D}}} ds\, df < \infty\end{aligned}$$

where we have made use of (5).

The ratio of the energy of the signal limited to the domain $\tilde{\mathcal{D}}$ to that of the original is $\mu(\tilde{\mathcal{D}}) = \langle (\mathcal{P}_{\tilde{\mathcal{D}}} x), (\mathcal{P}_{\tilde{\mathcal{D}}} x) \rangle / E_x$. Then, by the Hilbert–Schmidt theorem, there is a complete orthonormal basis $\{\psi_k(t)\}$ for $L^2(\mathbb{R})$ so that $(\mathcal{P}_{\tilde{\mathcal{D}}} \psi_k)(t) = \lambda_k \psi_k(t)$ and, as shown in Section II-A, when $E_x = 1$ the maximum energy is $\mu(\tilde{\mathcal{D}}) = \lambda_0^2$. The function $x(t)$ that maximizes $\mu(\tilde{\mathcal{D}})$ while retaining the normalization and such that $\langle \psi_k, x \rangle = 0$, $k = 0, \ldots, j-1$ is simply $\psi_j(t)$, and $\mu(\tilde{\mathcal{D}})$ is maximized at λ_j^2.

B. Area of Concentration

The resolution of identity can be rewritten in terms of the positive parameter a using (6)

$$x(t) = C_0 \int_{a\in\mathbb{R}^+} a^{-2} \left\{ \int_{b\in\mathbb{R}} \left[v_{a,b}^{(\beta,\gamma)}(t) \left\langle v_{a,b}^{(\beta,\gamma)}, x \right\rangle + v_{-a,-b}^{(\beta,\gamma)}(t) \left\langle v_{-a,-b}^{(\beta,\gamma)}, x \right\rangle \right] db \right\} da$$

or, because of (4) and (7), as

$$X(\nu) = C_0 \int_{a\in\mathbb{R}^+} a^{-2} \left\{ \int_{b\in\mathbb{R}} \left[V_{a,b}^{(\beta,\gamma)}(\nu) \left\langle V_{a,b}^{(\beta,\gamma)}, X \right\rangle + V_{a,b}^{(\beta,\gamma)}(-\nu) \left\langle V_{a,b}^{(\beta,\gamma)}(-), X \right\rangle \right] db \right\} da. \quad (8)$$

Then, in terms of $a \in \mathbb{R}^+$ and $b \in \mathbb{R}$, if we have

$$(a, b) \in \mathcal{A} \iff (s, f) \in \mathcal{D}$$

we can rewrite our operator as

$$(\mathcal{P}_{\mathcal{D}} x)(t) = C_0 \iint_{(a,b)\in\mathcal{A}} \left[v_{a,b}^{(\beta,\gamma)}(t) \left\langle v_{a,b}^{(\beta,\gamma)}, x \right\rangle + v_{-a,-b}^{(\beta,\gamma)}(t) \left\langle v_{-a,-b}^{(\beta,\gamma)}, x \right\rangle \right] db\, a^{-2} da.$$

The domain $\mathcal{D} \equiv \mathcal{D}_{C,\beta,\gamma}$ over which the operator $\mathcal{P}_{\mathcal{D}_{C,\beta,\gamma}}$ can be characterized [9, p. 678] is given by

$$\mathcal{D}_{C,\beta,\gamma} = \left\{ (s, f) \in \mathbb{R}^2 : \left(\frac{s}{C_2}\right)^2 \left(\frac{C_1}{|2\pi f|}\right)^{2\gamma-2} + \left(\frac{C_1}{|2\pi f|}\right)^{2\gamma} + 1 \le 2C \left(\frac{C_1}{|2\pi f|}\right)^{\gamma} \right\}$$

where C_1 and C_2 are

$$C_1 = \frac{2^{-1/\gamma}\Gamma\left(r + \frac{1}{\gamma}\right)}{\Gamma(r)};\ C_2 = \frac{\beta\gamma^{-1}2^{1/\gamma}\Gamma\left(r - \frac{1}{\gamma}\right)}{\Gamma(r)}.$$

The region $\mathcal{D}_{C,\beta,\gamma}$ consists of two parts symmetrically placed about the $f = 0$ line, but the region never includes $f = 0$ since a wavelet is a bandpass filter; the wavelet transform treats frequencies in a logarithmic fashion, and hence, $\mathcal{D}_{C,\beta,\gamma}$ cannot include zero frequency, however large C is.

Under the change of variables

$$a = C_1^{\gamma}[2\pi|f|]^{-\gamma};\ b = C_2^{-1} s\, a^{1-(1/\gamma)}$$

the set $\mathcal{D}_{C,\beta,\gamma}$ corresponds exactly to $|z - iC|^2 \le (C^2 - 1)$, i.e., $\mathcal{A} = \{(a, b) : a^2 + b^2 + 1 \le 2aC\}$ in the half-plane defined by $z = b + ia \in \mathbb{C}$, $\Im(z) = a > 0$.

The area of $\mathcal{D}_{C,\beta,\gamma}$ may be derived as

$$\begin{aligned}|\mathcal{D}_{C,\beta,\gamma}| &= 2\pi \iint_{(s,f)\in\mathcal{D}_{C,\beta,\gamma}} ds\, df \\ &= 2 \times \frac{C_1C_2}{\gamma} \iint_{a^2+b^2+1\le 2aC} a^{-2} da\, db \\ &= \frac{\Gamma\left(r+1-\frac{1}{\gamma}\right)\Gamma\left(r+\frac{1}{\gamma}\right)}{\gamma\Gamma^2(r)} \iint_{a^2+b^2+1\le 2aC} a^{-2} da\, db \\ &= \frac{2\pi(C-1)\Gamma\left(r+1-\frac{1}{\gamma}\right)\Gamma\left(r+\frac{1}{\gamma}\right)}{\gamma\Gamma^2(r)}.\end{aligned}$$

The factor of 2 takes into account that both the equal-sized positive and negative frequency segments of $\mathcal{D}_{C,\beta,\gamma}$ are mapped to $a^2 + b^2 + 1 \le 2aC$ with $a > 0$. We note that $\mathcal{D}_{C,\beta,\gamma} = 6\pi(C-1)$ when $\beta = \gamma = 1$, agreeing with this special case given in [9, eq. (3.11)].

When $s = 0$, b is also zero, and then, a satisfies

$$C - \sqrt{(C^2 - 1)} \le a \le C + \sqrt{(C^2 - 1)}.$$

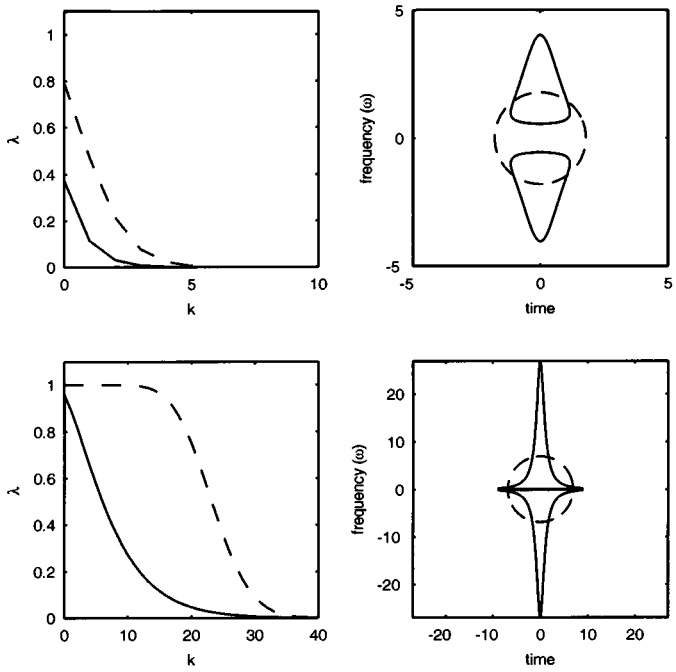

Fig. 1. Left: Hermite eigenvalues $\lambda_k(R)$ (dashed) and Morse eigenvalues $\lambda_{k;r}(C)$ for $\beta = \gamma = 1$ (solid) for domains of area 10 (top) and 150 (bottom). Right: Matching domains $\mathcal{D}_R$ and $\mathcal{D}_{C,1,1}$.

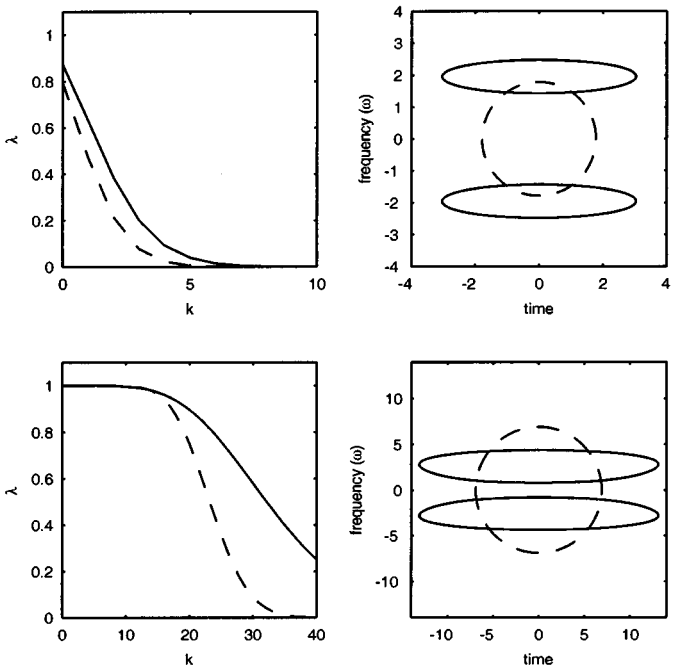

Fig. 2. Left: Hermite eigenvalues $\lambda_k(R)$ (dashed) and Morse eigenvalues $\lambda_{k;r}(C)$ for $\beta = 20, \gamma = 3$ (solid) for domains of area 10 (top) and 150 (bottom). Right: Matching domains $\mathcal{D}_R$ and $\mathcal{D}_{C,20,3}$.

For $f > 0$, we have $f = C_1/(2\pi a^{1/\gamma})$ so that

$$f_{\substack{\min\\\max}} = \frac{2^{-1/\gamma}\Gamma\left(r+\frac{1}{\gamma}\right)}{\left\{2\pi\Gamma(r)\left[C \pm \sqrt{(C^2-1)}\right]^{1/\gamma}\right\}}.$$

As $f > 0$ varies between $f_{\min}$ and $f_{\max}$, the corresponding s value on the boundary of $\mathcal{D}_{C,\beta,\gamma}$ is given by $s = bC_2a^{-1+(1/\gamma)}$, where $a = [C_1/(2\pi f)]^\gamma$, and $b = \sqrt{(2aC - 1 - a^2)}$. For $f < 0$, the boundary of the region is given by the obvious symmetry.

Fig. 1 shows the shapes of the domains $\mathcal{D}_R$ and $\mathcal{D}_{C,1,1}$ for domain areas of 10 and 150, whereas Fig. 2 compares $\mathcal{D}_R$ and $\mathcal{D}_{C,20,3}$.

C. Eigenvalues

The form of each eigenvalue of $\mathcal{P}_{\mathcal{D}_{C,\beta,\gamma}}$ depends on β and γ (through r) and on C. Unfortunately, the formula for the kth-order eigenvalues $\lambda_{k;r}(C)$, say, stated in [9, p. 680], is incorrect and may have led Bayram and Baraniuk [5, p. 306] to conclude that "no closed form expression exists for the eigenvalues for any choices of β and γ other than $\beta = \gamma = 1$." A rederivation shows that in fact

$$\lambda_{k;r}(C) = \frac{\Gamma(r+k)}{\Gamma(k+1)\Gamma(r-1)} \int_0^{(C-1)/(C+1)} x^k(1-x)^{r-2}dx.$$

The incomplete beta function is defined as [15, eqn. 6.6.1]

$$I_y(u,v) = \frac{\Gamma(u+v)}{\Gamma(u)\Gamma(v)} \int_0^y x^{u-1}(1-x)^{v-1}dx$$

so that $\lambda_{k;r}(C) = I_{(C-1)/(C+1)}(k+1, r-1)$. Further, when $r \geq 2$ is an integer, we can write [15, eqn. 25.5.7]

$$\lambda_{k;r}(C) = \left(\frac{C-1}{C+1}\right)^{k+r-1} \sum_{l=0}^{r-2} \binom{k+r-1}{l} \left(\frac{2}{C-1}\right)^l$$

agreeing with the special case $\beta = \gamma = 1$ (or $r = 3$) given in [9, eqn.4.6].

The energy concentration corresponding to the kth Hermite eigenfunction and the kth Morse eigenfunction is, as we have seen, given by the square of the kth eigenvalue. With $\beta = \gamma = 1$, which is the nongeneralized Morse case, we see in Fig. 1 that the Hermite eigenfunctions outperform the Morse ones, agreeing with [5]. However, it is easy to find many values of β and γ from the generalized Morse forms, for which the reverse is true: an example being $\beta = 20$ and $\gamma = 3$, as shown in Fig. 2. It is the property $\gamma > 1$ that is crucial to obtaining high energy concentrations, in particular, exceeding that of the Hermite eigenfunctions; therefore, the generalized Morse forms with $\gamma > 1$ are critically required for this reason.

D. Analytic and Anti-Analytic Eigenfunctions

The space $L^2(\mathbb{R})$ can be written as the direct sum of two closed subspaces $H_+^2(\mathbb{R})$ and $H_-^2(\mathbb{R})$

$$L^2(\mathbb{R}) = H_+^2(\mathbb{R}) \oplus H_-^2(\mathbb{R}). \tag{9}$$

Here, elements of the projection $L^2(\mathbb{R}) \to H_+^2(\mathbb{R})$ are defined by $x(t) \mapsto x(t)/2 + i\mathcal{H}\{x(t)/2\}$, and elements of the projection $L^2(\mathbb{R}) \to H_-^2(\mathbb{R})$ are defined by $x(t) \mapsto x(t)/2 - i\mathcal{H}\{x(t)/2\}$ [10, p. 28], where $\mathcal{H}\{\cdot\}$ denotes the Hilbert transform. We see that the subspace $H_+^2(\mathbb{R})$ contains "analytic signals," i.e., functions for which the imaginary part is the Hilbert transform of

the real part. A key property of an analytic signal is that its Fourier transform is supported by the positive frequencies only. The subspace $H^2_-(\mathbb{R})$ contains "anti-analytic signals," that are supported on the negative frequencies only.

The kth eigenvalue of $\mathcal{P}_{\mathcal{D}_{C,\beta,\gamma}}$ has multiplicity two with associated Hermitian eigenfunctions $\psi^+_{k;\beta,\gamma}(t)$, which is an analytic wavelet, and $\psi^-_{k;\beta,\gamma}(t)$, which is an anti-analytic wavelet, both of norm unity. The Fourier transforms of these functions are *real-valued* on the positive and negative frequency axes, respectively, with [9, p. 679]

$$\Psi^+_{k;\beta,\gamma}(f) = \sqrt{2}A_{k;\beta,\gamma}(2\pi f)^\beta e^{-(2\pi f)^\gamma} L_k^c\left(2[2\pi f]^\gamma\right) \quad (10)$$

for $f > 0$ and zero otherwise, and

$$\Psi^-_{k;\beta,\gamma}(f) = \sqrt{2}A_{k;\beta,\gamma}(2\pi|f|)^\beta e^{-(2\pi|f|)^\gamma} L_k^c\left(2[2\pi|f|]^\gamma\right)$$

for $f < 0$ and zero otherwise. Here, $c = r - 1$ and $A_{k;\beta,\gamma} = \sqrt{[\pi\gamma 2^r\Gamma(k+1)/\Gamma(k+r)]}$, and $L_k^c(\cdot)$ denotes the generalized Laguerre polynomial

$$L_k^c(x) = \sum_{m=0}^{k}(-1)^m \frac{\Gamma(k+c+1)}{\Gamma(c+m+1)\Gamma(k-m+1)}\frac{x^m}{m!}.$$

Notice that $\Psi^-_{k;\beta,\gamma}(f) = \Psi^+_{k;\beta,\gamma}(-f)$ and since the Fourier transforms are real, this means that $\psi^+_{k;\beta,\gamma}(t)$ and $\psi^-_{k;\beta,\gamma}(t)$ are complex conjugates, as expected. We will call $\psi^+_{k;\beta,\gamma}(t)$ and $\psi^-_{k;\beta,\gamma}(t)$ the kth-order generalized Morse eigenfunctions or wavelets.

E. Computation of $\psi^+_{k;\beta,\gamma}(t)$

To get a finely sampled representation of the complex wavelet $\psi^+_{k;\beta,\gamma}(t)$, we first find a frequency value f_0 that is up to twice as large as the frequency at which $\Psi^+_{k;\beta,\gamma}(f)$ dies down to zero. Next, define for N a suitably large power of 2 (such as 512)

$$C_l = \begin{cases} \Psi^+_{k;\beta,\gamma}\left(\frac{2f_0 l}{N}\right), & \text{for } l = 0,\ldots,\frac{N}{2} \\ 0, & \text{for } l = \frac{N}{2}+1,\ldots,M-1 \end{cases}$$

where $M = nN$ is a larger power of 2 than N, e.g., take $n = 4$. Then, for $m = 0,\ldots,M-1$, a periodic representation of the complex wavelet is given by

$$\psi^{+(p)}_{k;\beta,\gamma}(m\Delta t) = \frac{1}{M\Delta t}\sum_{l=0}^{M-1} C_l e^{i2\pi lm/M}$$

with $\Delta t = 1/(2nf_0)$. Since $\int_{\mathbb{R}}|\psi_{k;\beta,\gamma}(t)|^2dt = 1$, it is found that $\Delta t\sum_{m=0}^{M-1}[\psi^{+(p)}_{k;\beta,\gamma}(m\Delta t)]^2 \doteq 1$. Finally, $\psi^+_{k;\beta,\gamma}$ is found by rotating $\psi^{+(p)}_{k;\beta,\gamma}$ to be centered on zero, and $\psi^-_{k;\beta,\gamma}$ is found by complex conjugation.

IV. Generalized Morse Wavelets

A. CWT and Even and Odd Wavelets

The function to be analyzed $x(t)$ and the wavelet $\psi(t)$ are both assumed to be finite-energy functions, i.e., $x(t)$, $\psi(t) \in L^2(\mathbb{R})$. The continuous wavelet transform (CWT) is defined as [12, p. 24]

$$W(\tilde{a},b;x,\psi) = \frac{1}{\sqrt{|\tilde{a}|}}\int_{\mathbb{R}} x(t)\psi^*\left(\frac{t-b}{\tilde{a}}\right)dt, \quad \tilde{a},b \in \mathbb{R}.$$

Negative scales correspond to time-reversed wavelets, e.g., for $a > 0$

$$\frac{1}{\sqrt{a}}\psi\left(\frac{t-b}{-a}\right) = \frac{1}{\sqrt{a}}\psi\left(\frac{b-t}{a}\right).$$

We can write any wavelet as

$$\begin{aligned}\psi(t) =& \frac{1}{2}[\psi(t)+\psi(-t)] + \frac{1}{2}[\psi(t)-\psi(-t)] \\ =& \frac{1}{\sqrt{2}}\left[\psi^{(e)}(t)+\psi^{(o)}(t)\right], \text{ say}\end{aligned}$$

i.e., a sum of an even wavelet $\psi^{(e)}(t) = (1/\sqrt{2})[\psi(t)+\psi(-t)]$ and an odd wavelet $\psi^{(o)}(t) = (1/\sqrt{2})[\psi(t)-\psi(-t)]$. Reversing time when using an even wavelet has no effect, and thus, the odd part of the wavelet picks up any asymmetry in time. For the CWT with $a > 0$

$$\begin{aligned}W(a,b;x,\psi) =& \frac{1}{\sqrt{2}}\left[W\left(a,b;x,\psi^{(e)}\right)+W\left(a,b;x,\psi^{(o)}\right)\right] \\ W(-a,b;x,\psi) =& \frac{1}{\sqrt{2}}\left[W\left(a,b;x,\psi^{(e)}\right)-W\left(a,b;x,\psi^{(o)}\right)\right].\end{aligned}$$

$W(a,b;x,\psi)$ corresponds to time flowing in the same direction for x and ψ; $W(-a,b;x,\psi)$ corresponds to time flowing in opposite directions.

B. Generalized Morse Wavelets

The two kth-order generalized Morse eigenfunctions can be combined to give two real Morse wavelets—one even and one odd—for each eigenvalue, with Fourier transforms

$$\begin{aligned}\Psi^{(e)}_{k;\beta,\gamma}(f) =& \frac{1}{\sqrt{2}}\left[\Psi^+_{k;\beta,\gamma}(f)+\Psi^-_{k;\beta,\gamma}(f)\right] \\ \Psi^{(o)}_{k;\beta,\gamma}(f) =& \frac{1}{i\sqrt{2}}\left[\Psi^+_{k;\beta,\gamma}(f)-\Psi^-_{k;\beta,\gamma}(f)\right].\end{aligned}$$

The corresponding even and odd kth-order generalized Morse wavelets are given by

$$\begin{aligned}\psi^{(e)}_{k;\beta,\gamma}(t) =& 2\int_{\mathbb{R}^+}\Psi^{(e)}_{k;\beta,\gamma}(f)\cos(2\pi ft)df \\ \psi^{(o)}_{k;\beta,\gamma}(t) =& 2\int_{\mathbb{R}^+}\Psi^{(e)}_{k;\beta,\gamma}(f)\sin(2\pi ft)df\end{aligned}$$

with $\psi^{(e)}_{k;\beta,\gamma}(t)$, $\psi^{(o)}_{k;\beta,\gamma}(t) \in \mathbb{R}$, and analytic wavelet

$$\psi^+_{k;\beta,\gamma}(t) = \frac{1}{\sqrt{2}}\left[\psi^{(e)}_{k;\beta,\gamma}(t)+i\psi^{(o)}_{k;\beta,\gamma}(t)\right].$$

The real part of $\psi^+_{k;\beta,\gamma}(t)$ being even and the imaginary part being odd, of course, results in its Fourier transform $\Psi^+_{k;\beta,\gamma}(f)$ being real-valued, as already noted.

For a real function $x(t)$, the even and odd wavelet transform components can be recovered from the real and imaginary parts of the complex CWT.

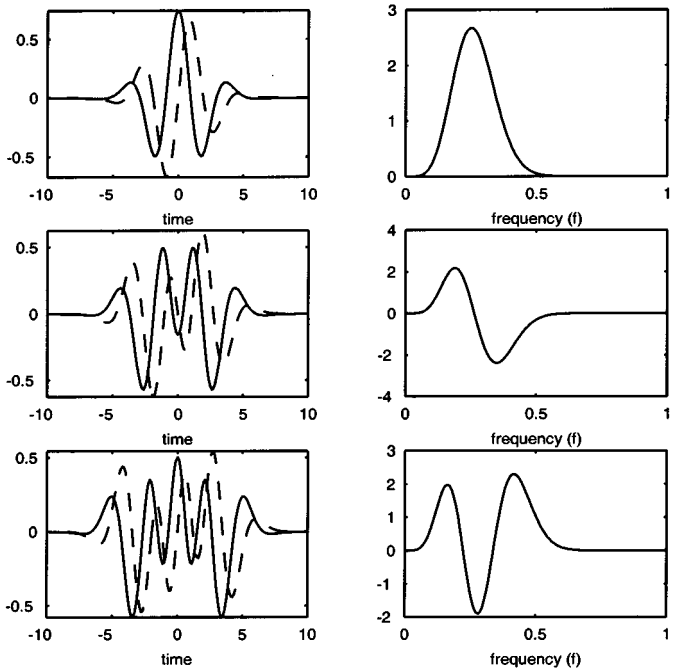

Fig. 3. Left: Even (solid) and odd (dashed) generalized Morse wavelets for $\beta = 5, \gamma = 2$, for (top) $k = 0$, (middle) $k = 1$, and (bottom) $k = 2$. Right: Corresponding frequency function $\Psi^{+}_{k;5,2}(f)$.

We have already obtained a partition of $L^2(\mathbb{R})$ in terms of the analytic and anti-analytic wavelets $\psi^{+}_{k;\beta,\gamma}(t)$ and $\psi^{-}_{k;\beta,\gamma}(t)$ [see (9)]. The even and odd wavelets $\psi^{(e)}_{k;\beta,\gamma}(t)$ and $\psi^{(o)}_{k;\beta,\gamma}(t)$ enable us to create a different orthogonal partition of $L^2(\mathbb{R})$, which can be considered to be the direct sum of a time direction invariant space (even functions) and a time direction sensitive space (odd functions). The advantage of this partition is that $\psi^{(e)}_{k;\beta,\gamma}(t)$ and $\psi^{(o)}_{k;\beta,\gamma}(t)$ are real functions. An example of even and odd generalized Morse wavelets is given for $\beta = 5$ and $\gamma = 2$ in Fig. 3, along with the corresponding frequency function defined in (10).

C. Time-Domain Eigenfunctions

For the special case of $\beta = 2m$, $m \in \mathbb{Z}^{+}$, and $\gamma = 2$, we can explicitly find the eigenfunctions in the time domain. We look at the case $k = 0$; for $k > 0$, the same approach can be used, but it will be more complicated. Consider

$$\begin{aligned}\psi^{(e)}_{0;2m,2}(t) &= \int_{\mathbb{R}} \Psi^{(e)}_{0;2m,2}(f) e^{i2\pi ft} df \\ &= 2\int_{\mathbb{R}^{+}} A_{0;2m,2}(2\pi f)^{2m} e^{-(2\pi f)^2} \cos(2\pi ft) df \\ &= \frac{2^{m+(3/4)}}{\sqrt{\{\pi\Gamma\left[2m+\frac{1}{2}\right]\}}} \int_{\mathbb{R}^{+}} \omega^{2m} e^{-\omega^2} \cos(\omega t) d\omega.\end{aligned}$$

We know from [16, sec.3.462] that

$$\int_{\mathbb{R}} (-1)^m x^{2m} e^{-x^2 - ixt} dx = 2^{-m}\sqrt{\pi} e^{-t^2/8} D_{2m}\left(\frac{t}{\sqrt{2}}\right)$$

where D_ν is the parabolic cylinder function. In addition, from [16, sec.9.253], we have $D_\nu(z) = 2^{-\nu/2} e^{-z^2/4} H_\nu(z/\sqrt{2})$, where H_ν are again the Hermite polynomials (see Section II-B). Hence

$$\begin{aligned}2^{-2m}\sqrt{\pi} e^{-t^2/4} H_{2m}\left(\frac{t}{2}\right) &= \int_{\mathbb{R}} (-1)^m x^{2m} e^{-x^2 - ixt} dx \\ &= 2\int_{\mathbb{R}^{+}} (-1)^m x^{2m} e^{-x^2} \cos(xt) dx\end{aligned}$$

so that

$$\psi^{(e)}_{0;2m,2}(t) = \frac{(-1)^m 2^{-[m+(1/4)]}}{\sqrt{\Gamma\left[2m+\left(\frac{1}{2}\right)\right]}} e^{-t^2/4} H_{2m}\left(\frac{t}{2}\right).$$

From (1), we can see that $\psi^{(e)}_{0;2m,2}(t)$ is proportional to $\exp(-t^2/8) h_{2m}(t/2)$, where $h_k(t)$ is the kth orthonormal Hermite eigenfunction introduced in Section II-B. A finely sampled version of $\psi^{(o)}_{0;2m,2}(t)$ can be computed by applying a numerical Hilbert transform (e.g., [17, p. 361]) to a finely sampled version of $\psi^{(e)}_{0;2m,2}(t)$.

V. Even, Odd, and Complex Wavelets and Scalograms

A. Eigenscalograms

For a set of wavelet eigenfunctions $\psi_k(t)$, $k = 0, \ldots, K-1$, we can define a multiple window time-varying spectrum estimate derived from a real-valued function $x(t)$ as the eigenscalogram [4], [5]

$$\hat{S}(a,b;x,\psi) = \frac{\sum_{k=0}^{K-1} d_k \left|W\left(a,b;x,\psi_k\right)\right|^2}{\sum_{k=0}^{K-1} d_k}$$

where the $\{d_k\}$ are weights. For example, using Morse wavelets, we could set $d_k = \lambda^2_{k;r}(C)$ (the energy concentration measure) for chosen values of β, γ (and, hence, r), and C.

B. Real Signals

Let $D = 1/\sum_k d_k$. Then, with $x(t)$ real-valued, the use of the complex-valued Morse wavelet $\psi^{+}_{k;\beta,\gamma}(t)$ means that

$$\begin{aligned}&W^*\left(a,b;x,\psi^{+}_k\right) W\left(a,b;x,\psi^{+}_k\right) \\ &\quad = W\left(a,b;x,\psi^{-}_k\right) W\left(a,b;x,\left[\psi^{-}_k\right]^*\right) \\ &\quad = W^*\left(a,b;x,\psi^{-}_k\right) W\left(a,b;x,\psi^{-}_k\right)\end{aligned}$$

so that

$$\begin{aligned}\hat{S}\left(a,b;x,\psi^{+}\right) &= D\sum_k d_k \Big\{\left|W\left(a,b;x,\psi^{+}_k\right)\right|^2 \\ &= \frac{D}{2}\sum_k d_k \Big\{\left|W\left(a,b;x,\psi^{+}_k\right)\right|^2 \\ &\qquad + \left|W\left(a,b;x,\psi^{-}_k\right)\right|^2\Big\} \\ &= \frac{1}{2}\left[\hat{S}\left(a,b;x,\psi^{+}\right) + \hat{S}\left(a,b;x,\psi^{-}\right)\right]\end{aligned}$$

so the eigenscalogram can be viewed as *implicitly* making use of both the $H^2_{+}(\mathbb{R})$ wavelet and the $H^2_{-}(\mathbb{R})$ wavelet. It is also straightforward to show that $\hat{S}(a,b;x,\psi^{+}_k)$ may be alternatively written as

$$\hat{S}\left(a,b;x,\psi^{+}_k\right) = \frac{1}{2}\left[\hat{S}\left(a,b;x,\psi^{(e)}\right) + \hat{S}\left(a,b;x,\psi^{(o)}\right)\right]$$

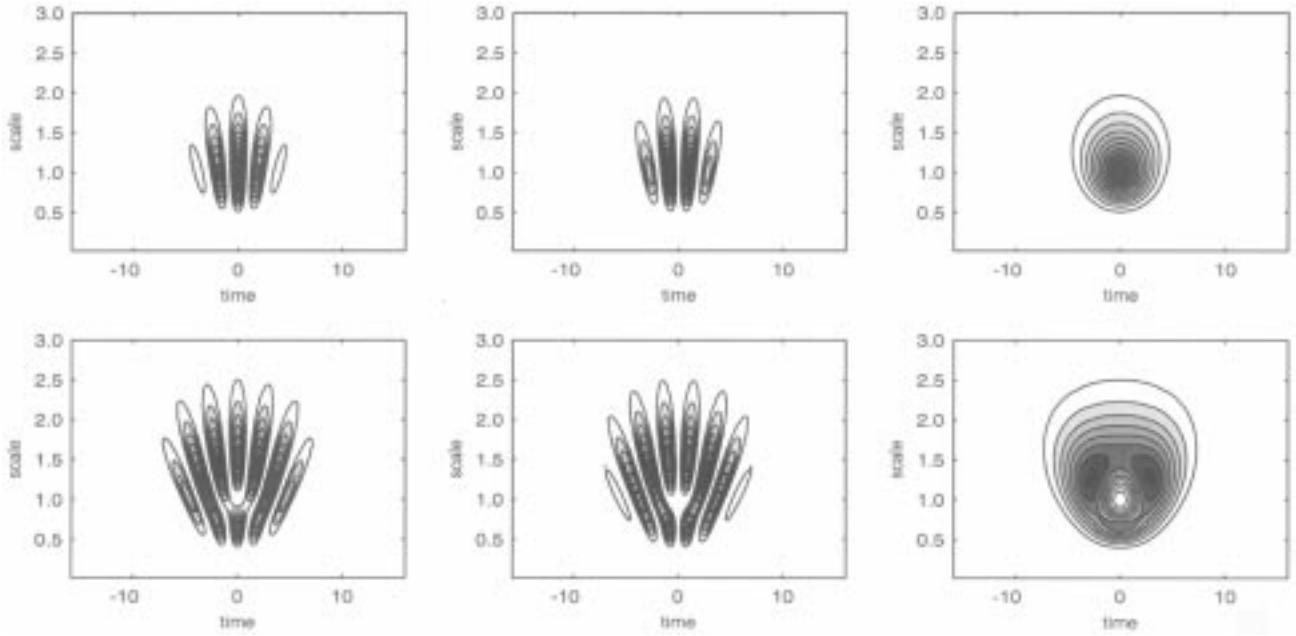

Fig. 4. Top row, left to right: $|W(a,b;x,\psi^{(e)}_{0;5,2})|^2$, $|W(a,b;x,\psi^{(o)}_{0;5,2})|^2$, and their sum. Bottom row, left to right: $|W(a,b;x,\psi^{(e)}_{1;5,2})|^2$, $|W(a,b;x,\psi^{(o)}_{1;5,2})|^2$, and their sum.

via the other partition of $L^2(\mathbb{R})$. Note for $x(t)$ real-valued

$$2\left|W\left(a,b;x,\psi^{+}_{k}\right)\right|^2 = \left|W\left(a,b;x,\psi^{(e)}_{k}\right)\right|^2 + \left|W\left(a,b;x,\psi^{(o)}_{k}\right)\right|^2.$$

The even/odd partition is illustrated in Fig. 4, which shows the analysis of the real-valued signal $x(t) = \psi^{(e)}_{0;5,2}(t)$ shown in Fig. 3. With weights of unity, the figure first shows (for order $k = 0$) $|W(a,b;x,\psi^{(e)}_{0;5,2})|^2$ and $|W(a,b;x,\psi^{(o)}_{0;5,2})|^2$, illustrating that the even and odd components occupy separate parts of time/scale space and, second, shows their sum, with energy distributed over a domain of form $\mathcal{A} = \{(a,b) : a^2 + b^2 + 1 \leq 2aC\}$ (see Section III-B). Corresponding plots for order $k = 1$ are also shown; we notice that because of the orthogonality of the eigenfunctions, there is now a "hole" at the point where the order $k = 0$ eigenscalogram showed highest energy concentration. The higher order also leads to more dissipated energy concentration.

C. Complex Signals

If $x(t)$ is complex-valued, i.e., $x(t) = x_R(t) + ix_I(t)$, say, then we find that in this case

$$\begin{aligned}&2\left|W\left(a,b;x,\psi^{+}_{k}\right)\right|^2\\ &= \left|W\left(a,b;x,\psi^{(e)}_{k}\right)\right|^2 + \left|W\left(a,b;x,\psi^{(o)}_{k}\right)\right|^2\\ &\quad + 2\Big[W\left(a,b;x_R,\psi^{(e)}_{k}\right)W\left(a,b;x_I,\psi^{(o)}_{k}\right)\\ &\qquad - W\left(a,b;x_I,\psi^{(e)}_{k}\right)W\left(a,b;x_R,\psi^{(o)}_{k}\right)\Big].\end{aligned}$$

This illustrates that when dealing with the most general form of signals (complex) and using orthogonal subspace representations, we need to make *explicit* use of both orthogonal components for $a > 0$. (Note that $\psi^{-}_{k}(t) = \psi^{+}_{k}(-t)$.) If $L^2(\mathbb{R})$ is the direct sum of two orthogonal subspaces, we can composite our eigenfunctions into

$$\psi_k(t) = \frac{1}{\sqrt{2}}\begin{bmatrix}\psi^{(1)}_{k}(t)\\ \psi^{(2)}_{k}(t)\end{bmatrix}.$$

For example, we could have

$$\psi_k(t) = \frac{1}{\sqrt{2}}\begin{bmatrix}\psi^{+}_{k;\beta,\gamma}(t)\\ \psi^{-}_{k;\beta,\gamma}(t)\end{bmatrix} \text{ or } \psi_k(t) = \frac{1}{\sqrt{2}}\begin{bmatrix}\psi^{(e)}_{k;\beta,\gamma}(t)\\ \psi^{(o)}_{k;\beta,\gamma}(t)\end{bmatrix}.$$

The integrated norm of $\psi_k(t)$ equals unity. We then consider a vector form of the CWT; for $a > 0$

$$\begin{aligned}\mathbf{W}_k(a,b;x,\psi) &= \frac{1}{\sqrt{(2a)}}\int_{\mathbb{R}} x(t)\begin{bmatrix}\psi^{*(1)}_{k}\left(\frac{t-b}{a}\right)\\ \psi^{*(2)}_{k}\left(\frac{t-b}{a}\right)\end{bmatrix}dt\\ &= \frac{1}{\sqrt{2}}\begin{bmatrix}W_k\left(a,b;x,\psi^{(1)}_{k}\right)\\ W_k\left(a,b;x,\psi^{(2)}_{k}\right)\end{bmatrix}.\end{aligned}$$

Now, the vector components here can be considered to be the function $x(t)$s contribution at each point (a, b) in each orthogonal subspace. These contributions are orthogonal and, hence, cannot be added. The scalogram at (a, b) can be considered to be the "energy" of the function $x(t)$ at (a, b). Therefore, if we have decomposed $x(t)$ into orthogonal subspaces of $L^2(\mathbb{R})$, then we must add each contribution of the energy. The energy is thus simply the norm squared of the vector $\mathbf{W}_k(a,b;x,\psi)$:

$$\hat{S}(a,b;x,\psi) = D\sum_{k=0}^{K-1} d_k \mathbf{W}^H_k(a,b;x,\psi)\mathbf{W}_k(a,b;x,\psi).$$

VI. Example

To illustrate the improved interpretability and lower variance resulting from using several wavelets in a scalogram computation, we consider the following model for the real-valued signal $x(t)$:

$$x(t) = |t - 64.5|^{-1} + |t - 180.5|^{-1} + 0.5Z(t)$$

where $Z(t)$ is Gaussian noise with mean zero and variance unity. One realization of 256 samples at unit sample interval starting

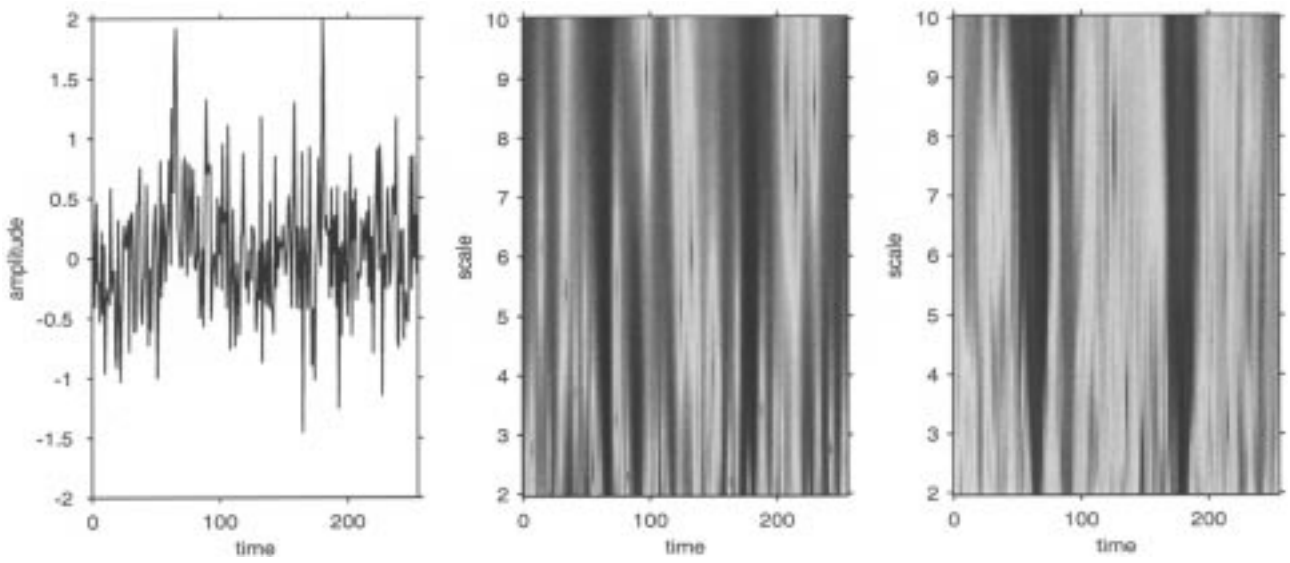

Fig. 5. From left to right, the noisy signal $x(t)$, $\log_{10}$ of the scalogram of the noisy signal using the single Morse wavelet $\psi^{+}_{0;\beta,\gamma}(t)$, and $\log_{10}$ of the average scalogram using the three Morse wavelets $\psi^{+}_{0;\beta,\gamma}(t)$, $\psi^{+}_{1;\beta,\gamma}(t)$, and $\psi^{+}_{2;\beta,\gamma}(t)$, with $\beta = 2$ and $\gamma = 1.1$.

from zero is shown in Fig. 5. The scalograms (on a $\log_{10}$ scale) of the noisy signal using the single Morse wavelet ψ^{+}_{0} and the simple average scalogram using the three Morse wavelets ψ^{+}_{0}, ψ^{+}_{1}, and ψ^{+}_{2} are also shown. The average scalogram using the multiple wavelets produces a much cleaner and more interpretable image, revealing the noise-free components of $x(t)$.

VII. Conclusions

Our results show that the GMWs have a considerable potential in digital signal processing. A set of orthogonal (eigenfunction) wavelets are exactly what is required for scalograms formed by weighted averaging. For complex signals, scalogram

$$
\begin{aligned}
&C_0 \iint_{(\tilde{a},b)\in\mathbb{R}^2} V^{(\beta,\gamma)}_{\tilde{a},b}(\nu)\left\langle V^{(\beta,\gamma)}_{\tilde{a},b}, X\right\rangle \tilde{a}^{-2}\,d\tilde{a}\,db \\
&= \mathcal{I}_{(\nu>0)} C' \int_{\mathbb{R}^+} \frac{d\nu_1}{2\pi} \int_{\mathbb{R}} db \int_{\mathbb{R}^+} d\tilde{a} \left\{ \frac{(2\tilde{a})^{r/2}}{\sqrt{\Gamma(r)}} \nu^{\beta} e^{-(\tilde{a}+ib)\nu^{\gamma}} \frac{(2\tilde{a})^{r/2}}{\sqrt{\Gamma(r)}} {\nu_1}^{\beta} e^{-(\tilde{a}-ib){\nu_1}^{\gamma}} X(\nu_1)\,\tilde{a}^{-2} \right\} \\
&\quad + \mathcal{I}_{(\nu<0)} C' \int_{\mathbb{R}^-} \frac{d\nu_1}{2\pi} \int_{\mathbb{R}} db \int_{\mathbb{R}^-} d\tilde{a} \left\{ \frac{(2|\tilde{a}|)^{r/2}}{\sqrt{\Gamma(r)}} |\nu|^{\beta} e^{-(\tilde{a}+ib)\nu|\nu|^{\gamma-1}} \frac{(2|\tilde{a}|)^{r/2}}{\sqrt{\Gamma(r)}} |\nu_1|^{\beta} e^{-(\tilde{a}-ib)\nu_1|\nu_1|^{\gamma-1}} X(\nu_1)\,\tilde{a}^{-2} \right\} \\
&= \mathcal{I}_{(\nu>0)} C_0 \int_{\mathbb{R}^+} ds \int_{\mathbb{R}} db \int_{\mathbb{R}^+} d\tilde{a} \left\{ \frac{(2\tilde{a})^{r}}{\Gamma(r)} \nu^{\beta} e^{-(\tilde{a}+ib)\nu^{\gamma}} e^{-(\tilde{a}-ib)s} s^{\beta/\gamma} X\left(s^{1/\gamma}\right) s^{(1/\gamma)-1} \tilde{a}^{-2} \right\} \\
&+ \mathcal{I}_{(\nu<0)} C_0 \int_{\mathbb{R}^-} ds \int_{\mathbb{R}} db \int_{\mathbb{R}^-} d\tilde{a} \left\{ \frac{(2|\tilde{a}|)^{r}}{\Gamma(r)} |\nu|^{\beta} e^{-(\tilde{a}+ib)\nu|\nu|^{\gamma-1}} e^{-(\tilde{a}-ib)s} |s|^{\beta/\gamma} X\left(s|s|^{(1/\gamma)-1}\right) |s|^{1/\gamma-1} \tilde{a}^{-2} \right\} \\
&= \mathcal{I}_{(\nu>0)} C_0 \int_{\mathbb{R}^+} ds \int_{\mathbb{R}^+} d\tilde{a} \left\{ \frac{(2\tilde{a})^{r}}{\Gamma(r)} \nu^{\beta} e^{-\tilde{a}\nu^{\gamma}} e^{-\tilde{a}s} s^{\beta/\gamma} 2\pi\delta(s-\nu^{\gamma}) X\left(s^{1/\gamma}\right) s^{(1/\gamma)-1} \tilde{a}^{-2} \right\} \\
&+ \mathcal{I}_{(\nu<0)} C_0 \int_{\mathbb{R}^-} ds \int_{\mathbb{R}^-} d\tilde{a} \left\{ \frac{(2|\tilde{a}|)^{r}}{\Gamma(r)} |\nu|^{\beta} e^{-\tilde{a}\nu|\nu|^{\gamma-1}} e^{-\tilde{a}s} |s|^{\beta/\gamma} 2\pi\delta(s-\nu|\nu|^{\gamma-1}) X\left(s|s|^{1/\gamma-1}\right) |s|^{1/\gamma-1} \tilde{a}^{-2} \right\} \\
&= \mathcal{I}_{(\nu>0)} C_0 \int_{\mathbb{R}^+} \left\{ \frac{(2\tilde{a})^{r}}{\Gamma(r)} \nu^{\beta} e^{-\tilde{a}\nu^{\gamma}} e^{-\tilde{a}\nu^{\gamma}} \nu^{\beta} 2\pi X(\nu) \nu^{1-\gamma} \tilde{a}^{-2} \right\} d\tilde{a} \\
&+ \mathcal{I}_{(\nu<0)} C_0 \int_{\mathbb{R}^-} \left\{ \frac{(2|\tilde{a}|)^{r}}{\Gamma(r)} |\nu|^{\beta} e^{-\tilde{a}\nu|\nu|^{\gamma-1}} e^{-\tilde{a}\nu|\nu|^{\gamma-1}} |\nu|^{\beta} 2\pi X(\nu) |\nu|^{1-\gamma} \tilde{a}^{-2} \right\} d\tilde{a} \\
&= C_0 \frac{2^r}{\Gamma(r)} |\nu|^{r\gamma-\gamma} 2\pi X(\nu) \int_{\mathbb{R}^+} e^{-2\tilde{a}|\nu|^{\gamma}} \tilde{a}^{r-2}\,d\tilde{a} \\
&= C_0 \frac{2^r}{\Gamma(r)} |\nu|^{r\gamma-\gamma} 2\pi X(\nu) \Gamma(r-1) \left(2|\nu|^{\gamma}\right)^{-(r-1)} \\
&= X(\nu), \quad \nu \in \mathbb{R}
\end{aligned}
$$

analyzes must be carried out using both the analytic and anti-analytic complex wavelets or odd and even real wavelets, whereas for real signals, the complex analytic wavelet is sufficient. The wavelets are easy to compute using the DFT and, for $(\beta,\gamma)=(2m,2)$, can be computed exactly. Our correction of the previously published eigenvalue formula shows that for $\gamma>1$, they can outperform the Hermites in energy concentration.

The complex nature of the wavelets makes them ideal for analyzing phase relationships in vector-valued or multicomponent time series [11].

Appendix
Resolution of Identity

Recall that $V_{\tilde{a},b}^{(\beta,\gamma)}(\nu)$ is defined as

$$\begin{cases} \frac{2^{(r/2)+(1/2)}\sqrt{[\pi\gamma]}|\tilde{a}|^{r/2}}{\sqrt{\Gamma(r)}}|\nu|^{\beta}e^{-(\tilde{a}+ib)\nu|\nu|^{\gamma-1}}, & \text{if } \tilde{a}\nu\in\mathbb{R}^{+} \\ 0, & \text{otherwise.} \end{cases}$$

Hence, our integral over $\mathbb{R}^2$ in ν and $\tilde{a}$ will collapse to two integrals: one over $\mathbb{R}^{+2}$ in ν and $\tilde{a}$ and one over $\mathbb{R}^{-2}$ in ν and $\tilde{a}$. Let$C'=2\pi\gamma C_0$, where $C_0=(2\beta+1-\gamma)/(4\gamma\pi)$. Then, we have the equation at the bottom of the previous page, and the last integral follows from [16, eqn.3.478(1)].

Acknowledgment

Helpful comments by a referee were much appreciated.

References

[1] D. J. Thomson, "Spectrum estimation and harmonic analysis," *Proc. IEEE*, vol. 70, pp. 1055–1096, 1982.
[2] G. Frazer and B. Boashash, "Multiple window spectrogram and time-frequency distributions," in *Proc. ICASSP*, vol. IV, 1994, pp. 293–6.
[3] P. Flandrin, *Time-Frequency/Time-Scale Analysis*. San Diego, CA: Academic, 1999.
[4] M. Bayram and R. Baraniuk, "Multiple window time-frequency analysis," in *Proc. IEEE Int. Symp. Time-Freq. Time-Scale Anal.*, Paris, France, 1996, pp. 511–14.
[5] ——, "Multiple window time-varying spectrum estimation," in *Nonlinear and Nonstationary Signal Processing*, W. J. Fitzgerald, R. L. Smith, A. T. Walden, and P. C. Young, Eds. Cambridge, U.K.: Cambridge Univ. Press, 2000, pp. 292–316.
[6] I. Daubechies, "Time-frequency localization operators: A geometric phase space approach," *IEEE Trans. Inform. Theory*, vol. 34, pp. 605–612, July 1988.
[7] P. Flandrin, "Maximum signal energy concentration in a time-frequency domain," in *Proc. ICASSP*, vol. IV, 1988, pp. 2176–9.
[8] T. W. Parks and R. G. Shenoy, "Time-frequency concentrated basis functions," in *Proc. ICASSP*, vol. V, 1990, pp. 2459–62.
[9] I. Daubechies and T. Paul, "Time-frequency localization operators—A geometric phase space approach: II. The use of dilations," *Inverse Problems*, vol. 4, pp. 661–680, 1988.
[10] M. Holschneider, *Wavelets: An Analysis Tool*. Oxford, U.K.: Oxford Univ. Press, 1995.
[11] S. Olhede and A. T. Walden, "Polarization phase relationships via multiple Morse wavelets—Part I: Fundamentals," *Proc. R. Soc. Lond., A*, 2002, to be published.
[12] I. Daubechies, *Ten Lectures on Wavelets*. Philadelphia, PA: SIAM, 1992.
[13] M. Reed and B. Simon, *Methods of Modern Mathematical Physics: 1 Functional Analysis*. New York: Academic, 1972.
[14] R. Courant and D. Hilbert, *Methods of Mathematical Physics*. New York: Wiley, 1953, vol. 1.
[15] M. Abramowitz and I. A. Stegun, *Handbook of Mathematical Functions*. New York: Dover, 1965.
[16] I. S. Gradshteyn and I. M. Ryzhik, *Table of Integrals, Series and Products (Corrected and Enlarged Edition)*. New York: Academic, 1980.
[17] A. V. Oppenheim and R. W. Schafer, *Digital Signal Processing*. Englewood Cliffs, NJ: Prentice-Hall, 1975.

Sofia C. Olhede received the M.Sci. degree in mathematics from Imperial College, London, U.K., in 2000. She is currently Beit Scientific Research fellow and is pursuing the Ph.D. degree at Imperial College.

Her research interests include time–frequency analysis and nonstationary time series.

Andrew T. Walden (AM'86) received the B.Sc. degree in mathematics from the University of Wales, Bangor, U.K., in 1977 and the M.Sc. and Ph.D. degrees in statistics from the University of Southampton, Southampton, U.K., in 1979 and 1982, respectively.

He was a research scientist at British Petroleum from 1981 to 1990, specializing in statistical signal processing for oil and gas exploration. From 1985 to 1986, he was a Visiting Assistant Professor with the University of Washington, Seattle, teaching and researching in both the Statistics and Geophysics Departments. He joined the Department of Mathematics at Imperial College, London, U.K., in 1990, where he is currently Professor of statistics. His research interests are in time series, spectrum analysis, and wavelets, particularly with applications to geophysics and oceanography. He is coauthor of the recent texts (with D. Percival) *Spectral Analysis for Physical Applications* and *Wavelet Methods for Time Series Analysis*.